Plant Cell Advance Publication. Published on February 1, 2019, doi:10.1105/tpc.18.00693

RESEARCH ARTICLE

The Histone H3K4 Demethylase JMJ16 Represses Leaf Senescence in Arabidopsis

Peng Liu,[a,1,2] Shuaibin Zhang,[b,1] Bing Zhou,[c,1] Xi Luo,[d] Xiao Feng Zhou,[e] Bin Cai,[a] Yin Hua Jin,[a] De Niu,[a] Jinxing Lin,[f] Xiaofeng Cao,[b,g,h,3] and Jing Bo Jin[a,3]

[a]Key Laboratory of Plant Molecular Physiology, Institute of Botany, Chinese Academy of Sciences, Beijing 100093, China，[b]State Key Laboratory of Plant Genomics and National Center for Plant Gene Research, Institute of Genetics and Developmental Biology, Chinese Academy of Sciences, Beijing 100101, China，[c]State Key Laboratory of Stem Cell and Reproductive Biology, Institute of Zoology, Chinese Academy of Sciences, Beijing 100101, China, [d]College of Life Sciences, Capital Normal University, Beijing 100048, China, [e]Department of Ornamental Horticulture, China Agricultural University, Beijing 100193, China, [f]China College of Biological Sciences and Biotechnology, Beijing Forestry University, Beijing 100083, China, [g]University of Chinese Academy of Sciences, Beijing 100049, China, [h]CAS Center for Excellence in Molecular Plant Sciences, Institute of Genetics and Developmental Biology, Chinese Academy of Sciences, Beijing 100101, China.
[1]These authors contributed equally to this work.
[2]Current address: Division of Biological Environmental Sciences and Engineering, King Abdullah University of Science and Technology, Thuwal, Saudi Arabia.
[3]Corresponding Authors: jinjb@ibcas.ac.cn and xfcao@genetics.ac.cn

Short title: Epigenetic regulation of leaf senescence

One-sentence summary: Age-dependent downregulation of JMJ16, a specific H3K4 demethylase, is required for epigenetic reprograming of senescence-associated gene expression during leaf senescence.

The authors responsible for distribution of materials integral to the findings presented in this article in accordance with the policy described in the Instructions for Authors (www.plantcell.org) are: Jing Bo Jin (jinjb@ibcas.ac.cn) and Xiaofeng Cao (xfcao@genetics.ac.cn).

ABSTRACT

Leaf senescence is governed by a complex regulatory network involving the dynamic reprogramming of gene expression. Age-dependent induction of senescence-associated genes (SAGs) is associated with increased levels of trimethylation of histone H3 at lysine 4 (H3K4me3), but the regulatory mechanism remains elusive. Here, we found that JMJ16, an *Arabidopsis thaliana* JmjC-domain

containing protein, is a specific H3K4 demethylase that negatively regulates leaf senescence through its enzymatic activity. Genome-wide analysis revealed a widespread coordinated up-regulation of gene expression and hyper-methylation of H3K4me3 at JMJ16-binding genes associated with leaf senescence in the loss-of-function *jmj16* mutant compared to the wild type. Genetic analysis indicated that JMJ16 negatively regulates leaf senescence, at least partly through repressing the expression of positive regulators of leaf senescence, *WRKY53* and *SAG201*. JMJ16 associates with *WRKY53* and *SAG201* and represses their precocious expression in mature leaves by reducing H3K4me3 levels at these loci. The protein abundance of JMJ16 gradually decreases during aging, which is correlated with increased H3K4me3 levels at *WRKY53* and *SAG201*, suggesting that the age-dependent down-regulation of JMJ16 is required for the precise transcriptional activation of SAGs during leaf senescence. Thus, JMJ16 is an important regulator of leaf senescence that demethylates H3K4 at SAGs in an age-dependent manner.

INTRODUCTION

Leaf senescence is the highly ordered final stage of leaf development. This process is characterized by the degradation of chlorophylls, nucleic acids, lipids, proteins, and other macromolecules, and subsequently by programmed cell death and changes in leaf color (Lim et al., 2007). The nutrients released during leaf senescence are recycled to reproductive organs or actively growing young tissues (Woo et al., 2013). Genome-wide transcriptional analyses revealed that dramatic changes in the expression of thousands of senescence-associated genes (SAGs) occur during leaf senescence; however, it is unclear how the transcriptional reprogramming of these genes is regulated in a time-dependent manner (Li et al., 2012; 2014).

Various transcription factors, including NAC (NAM, ATAF, CUC), WRKY, MYB, C2H2 zinc finger, bZIP (BASIC LEUCINE ZIPPER), and AP2 (APETALA2)/EREBP (ETHYLENE-RESPONSIVE ELEMENT-BINDING PROTEIN) family proteins, play pivotal roles in the transcriptional regulation of SAGs during leaf senescence in *Arabidopsis thaliana* (Balazadeh et al., 2008). However, the expression of the genes encoding these transcription factors is also regulated during leaf senescence, indicating that additional mechanisms determine the onset of leaf senescence (Woo et al., 2013). For example, ORESARA1 (ORE1, also

known as ANAC092), a NAC transcription factor, positively regulates leaf senescence (Kim et al., 2009). *ORE1* expression increases during leaf aging, and this increase is associated with an age-dependent, EIN2 (ETHYLENE-INSENSITIVE PROTEIN2)-mediated decline in transcription of the microRNA miR164 (Kim et al., 2009). Furthermore, WRKY53, a WRKY transcription factor, promotes leaf senescence by regulating the expression of its target genes, including *WRKY6*, *WRKY22,* and *ORE9* (Miao et al., 2004; Robatzek and Somssich, 2002; Woo et al., 2001; Zhou et al., 2011). *WRKY53* expression increases at the onset of senescence but is maintained at low levels before senescence (Ay et al., 2009). The age-dependent induction of *WRKY53* transcription is regulated by WHIRLY1 (WHY1), which directly binds to the promoter region of *WRKY53* and represses its expression (Miao et al., 2013; Huang et al., 2018). During leaf senescence, WHY1 gradually dissociates from the *WRKY53* promoter, and *WRKY53* transcription is subsequently induced (Miao et al., 2013). In addition, the induction of *WRKY53* expression during senescence is associated with increased trimethylation of histone H3 at lysine 4 (H3K4me3, a mark of actively transcribed chromatin) levels at the 5' end and coding region of *WRKY53* (Ay et al., 2009; Zhang et al., 2009). Genome-wide analysis of changes in histone methylation during senescence revealed that a large proportion of up-regulated SAGs are also associated with increased H3K4me3 levels (Brusslan et al., 2012). However, how the H3K4me3 levels at *WRKY53* and other SAGs are regulated remains largely unknown.

Overexpression of SU(VAR)3-9 homolog SUVH2, which is involved in RNA-directed DNA methylation, represses the expression of *WRKY53* and other SAGs by promoting ectopic H3K27me2/3 modifications (Ay et al., 2009; Liu et al., 2014; Jing et al., 2016). However, the repression of *WRKY53* expression prior to senescence is not associated with silencing chromatin marks (such as H3K9me2 and H3K27me3) in the wild type, suggesting that increased H3K4me3 levels, rather than decreased levels of silencing chromatin marks, underlie *WRKY53* activation in the

wild type (Ay et al., 2009). H3K4me3 methyltransferases and/or demethylases might regulate the age-dependent dynamic regulation of H3K4me3 levels at *WRKY53* and other SAGs, but this remains to be elucidated (Yolcu et al., 2018). The Arabidopsis genome contains six genes encoding homologs of lysine demethylase 5 (KDM5), including JMJ14, JMJ15, JMJ16, JMJ17, JMJ18, and JMJ19 (Lu et al., 2008). Among these, JMJ14, JMJ15, and JMJ18 have been shown to function as H3K4 demethylases that regulate the transition to flowering (Lu et al., 2010; Yang et al., 2012a; 2012b). However, the enzyme activities and functions of the other Arabidopsis KDM5 group members have not been characterized.

In the current study, we demonstrated that Arabidopsis JMJ16 is a specific H3K4 demethylase that negatively regulates age-dependent leaf senescence through its demethylase activity. Genome-wide analyses demonstrated that a loss-of-function mutation in JMJ16 increases H3K4me3 levels and induces the expression of numerous SAGs. Genetic and molecular analyses indicated that precociously increased H3K4me3 levels in *jmj16* mutants at *WRKY53* and *SAG201*, two known positive regulators of leaf senescence (Miao et al., 2004; Hou et al., 2013), are responsible for the early-senescence phenotype. Finally, we detected substantially reduced levels of JMJ16 during the late stages of leaf development, which may be responsible for the transcriptional activation of these SAGs. Together, these findings uncover a mechanism by which an H3K4 demethylase regulates the transcriptional reprogramming of SAGs during senescence by modulating H3K4me3 levels in an age-dependent manner.

RESULTS

JMJ16 represses leaf senescence

JMJ16 (also known as PKDM7D) is a member of the KDM5 group of proteins, which mediate demethylation of mono-, di-, and trimethylated H3K4 (H3K4me1/2/3) in humans (Lu et al., 2008). We found that *jmj16* loss-of-function mutants (Supplemental Figure 1A and 1B) accumulated higher levels of ROS (reactive oxygen

species) than wild type (Supplemental Figure 1D and 1E). Since increased ROS levels and dynamic changes in H3K4 methylation homeostasis are often associated with leaf senescence in Arabidopsis (Woo et al., 2013; Ay et al., 2009; Brusslan et al., 2012; Pan et al., 2018), we speculated that *JMJ16* might regulate leaf senescence. Consistent with our speculation, we observed an early leaf senescence phenotype in 6.5-week-old *jmj16* T-DNA insertion mutant lines grown under long-day conditions, i.e., *jmj16-1*, *-2,* and *-3*, but not in the wild type (Figure 1A; left panel). The early leaf senescence phenotype of the *jmj16* mutants was even more pronounced in 8-week-old plants grown under long days (Figure 1A; right panel). On the other hand, mutations in other KDM5 family genes, including *JMJ14*, *JMJ17*, and *JMJ18*, did not lead to altered leaf senescence (Supplemental Figure 2). Moreover, the chlorophyll content and photochemical efficiency of photosystem II (Fv/Fm), two physiological parameters that decrease during leaf senescence (Oh et al., 1996), were lower in the *jmj16* mutants compared to the wild type (Figure 1B and 1C). In addition, the expression of the senescence-associated gene *SAG12* was up-regulated in leaves 5 and 6 of 6.5-week-old *jmj16* plants, but not in the wild type (Figure 1D). Genetic transformation of *jmj16-1* with *JMJ16* genomic DNA completely rescued its early-senescence phenotype (Figure 1E; Supplemental Figure 3A, 3C and 3D). These results indicate that JMJ16 represses leaf senescence. In addition to the early-senescence phenotype, the *jmj16* mutants exhibited silique abortion, which was also rescued by the expression of *JMJ16* (Figure 1F; Supplemental Figure 3B). We also noticed that the *jmj16* mutants exhibited slightly earlier flowering than the wild type (Supplemental Figure 1F). Although the *jmj14* mutation causes early flowering (Lu et al., 2010), it did not affect leaf senescence (Supplemental Figure 2A). Thus, it is unlikely that the slightly accelerated transition to flowering causes the strikingly early leaf senescence of *jmj16*.

JMJ16 specifically demethylates H3K4 methylation

To examine the histone demethylase activity of JMJ16, we transiently expressed

JMJ16-YFP-HA in wild tobacco (*Nicotiana benthamiana*) leaves and compared the histone modification levels in transfected and non-transfected cells, as previously described (Lu et al., 2010). In JMJ16-YFP-HA-expressing cells, H3K4me1/2/3 signals were substantially reduced (Figure 2A and 2C), whereas mono-, di-, or trimethylation levels at H3K9, H3K27, and H3K36 were not affected (Supplemental Figure 4A). Transient expression of JMJ16m-YFP-HA, in which His381 and Glu383 (two conserved iron-binding amino acids) of JMJ16 were replaced with alanine, abolished the H3K4 demethylase activity, indicating that the conserved iron-binding amino acids are critical for the H3K4 demethylase activity of JMJ16 (Figure 2B and 2C).

We then measured the H3K4 demethylase activity of JMJ16 in vitro as described previously (Yang et al., 2010). Similar to GST-JMJ14$_{596}$ (Yang et al., 2010), affinity purified recombinant protein GST-JMJ16$_{670}$ (A 670 amino acid fragment of JMJ16 containing the JmjN, JmjC and C5HC2 zinc finger domains) exhibited demethylation activity for mono-, di-, and trimethylated H3K4, but not for H3K9, H3K27 or H3K36, in vitro (Figure 2D; Supplemental Figure 4B). To confirm that JMJ16 has H3K4 demethylase activity in Arabidopsis, we generated transgenic Col-0 plants overexpressing JMJ16-YFP-HA (referred to as *JMJ16 OE*; Supplemental Figure 5), and examined the global mono-, di-, and trimethylation levels at H3K4. Overexpression of JMJ16-YFP-HA caused a globally decrease in di- and trimethylation but an increase in monomethylation levels at H3K4, which is similar to what was observed for JMJ14-YFP-HA overexpression (Figure 2E and 2F). The global hypermethylation of H3K4me1 in JMJ16-YFP-HA overexpression plants might have occurred because the expression level of JMJ16 was not sufficient to catalyze the formation of enriched monomethylated H3K4 due to elevated demethylation of H3K4me2/3 in these plants. Taken together, these results indicate that JMJ16 is an H3K4-specific demethylase in Arabidopsis.

JMJ16 negatively regulates the transcription and H3K4me3 levels of its target genes

Since JMJ16 is an H3K4me3 demethylase (Figure 2) and H3K4me3 is associated with active gene transcription (Zhang et al., 2009), we wanted to evaluate the direct effect of depletion of JMJ16 on the transcription of its target genes. To identify JMJ16-regulated genes at the genome-wide scale, we sequenced RNA from leaves 5 and 6 of 5-week-old wild type and *jmj16-1* plants (Supplemental Data Set 1). At this stage, the leaves were in the mature stage and fully expanded and exhibited no visible yellowing in either the wild type or *jmj16-1* mutant. A total of 10.6 million (65.3%) and 13.8 million (73.8%) clean reads were uniquely aligned to the Arabidopsis reference genome, which were mapped to 15,988 and 15,842 genes in the wild type and *jmj16-1*, respectively (TPM (Transcripts Per Kilobase Million) > 1). Among these, 3,355 genes were up-regulated (fold change > 1.5) and 2,594 genes were down-regulated (fold change > 1.5) in *jmj16-1* compared with the wild type (Supplemental Data Set 1).

To investigate whether these up-regulated genes in *jmj16-1* are directly associated targets of JMJ16, we performed chromatin immunoprecipitation followed by sequencing (ChIP-seq) to capture genome-wide direct binding targets of JMJ16. A construct containing *JMJ16-HA* driven by the *JMJ16* promoter was transformed into *jmj16-1* (Supplemental Figure 6A to 6C). The expression of JMJ16-HA rescued the early-senescence phenotype of *jmj16-1*, indicating that the HA fusion proteins were functional (Figure 3A). We performed ChIP-seq with anti-HA antibody in the leaves of *jmj16-1* (as a negative control) and *JMJ16-HA* transgenic plants of the same stage as those used in RNA-seq and identified 1,111 up-regulated genes with significantly enriched binding (fold change > 2) in *jmj16-1* harboring JMJ16-HA (Figure 4A; Supplemental Data Set 2). These results indicate that highly up-regulated genes in *jmj16-1* are direct targets of JMJ16.

Since the homeostasis of H3K4me3 is dynamically maintained by the synergistic effects of members of the methyltransferase and demethylase families, we were interested in investigating whether the up-regulation of these JMJ16 target genes exhibited significant changes in H3K4me3 modification at these loci. Thus, we performed ChIP-seq using the anti-H3K4me3 antibody to identify genome-wide hyper-methylated H3K4me3 loci in wild-type and *jmj16-1* leaves of the same stage as those used in RNA-seq. In the *jmj16-1* mutant, H3K4me3 levels were increased at least 1.5-fold for 4,539 genes compared with the wild type (Supplemental Data Set 3). Among the 1,111 JMJ16 binding targets and transcriptionally up-regulated genes in *jmj16-1*, 370 genes exhibited hyper-methylation (fold change > 2) of H3K4me3 compared with the wild type (Figure 4A; Supplemental Data Set 4). These results suggest that JMJ16 directly is associated with these 370 genes and dominantly regulates H3K4me3 levels at these loci in wild-type plants. In *jmj16-1* plants, the depletion of JMJ16 led to enhanced H3K4me3 levels at these loci, which subsequently up-regulated the expression of these genes. Meta-gene analysis clearly revealed increased H3K4me3 levels, especially at transcription start site (TSS) regions, due to the depletion of JMJ16 in *jmj16-1* (Figure 4D and 4F). Interestingly, the direct JMJ16 binding regions of genes with enhanced H3K4me3 levels were enriched in both the gene bodies and TSS regions (Figure 4E and 4F). Together, these results strongly support the notion that JMJ16 primarily regulates gene expression through the direct regulation of H3K4me3 levels in wild-type plants.

A comparison of JMJ16-associated genes and H3K4me3-hypermethylated genes in *jmj16-1* with genes listed in the LSD 2.0 leaf senescence database (Li et al., 2014) revealed that 325 genes were senescence-associated genes (Figure 4B; Supplemental Data Set 5). Of the 325 H3K4me3 hypermethylated SAGs that were associated with JMJ16, 138 were transcriptionally up-regulated in *jmj16-1* (Figure 4C; Supplemental Data Set 4). We selected five of these 138 overlapping SAGs to validate the RNA-seq and ChIP-seq results. RT-qPCR and ChIP-qPCR analysis confirmed the up-regulated

185 expression and increased H3K4me3 levels of all five genes, i.e., transcription factor
186 gene *WRKY53*, *SAG201*, *SAG13*, Cysteine-Rich Receptor-Like Kinase gene *CRK36,*
187 and transmembrane protein gene At5g20790 in 5-week-old *jmj16-1* plants compared
188 with the wild type (Figure 4G to 4I and 4K to 4M; Supplemental Figure 7). These five
189 genes include two genes encoding known positive regulators of leaf senescence,
190 *WRKY53* (Miao et al., 2004) and *SAG201* (also known as *SAUR36*) (Hou et al., 2013),
191 as well as *SAG13*, *CRK36,* and At5g20790, which were all identified as JMJ16-target
192 genes (Supplemental Data Set 4). ChIP-qPCR analysis confirmed that JMJ16-HA was
193 directly associated with the chromatin regions of these genes (Figure 4J and 4N;
194 Supplemental Figure 7D, 7H and 7L).

195 **The early-senescence phenotype of *jmj16* is at least partly due to up-regulated**
196 ***WRKY53* and *SAG201* expression**

197 To determine if the early-senescence phenotype of *jmj16-1* is associated with
198 increased *WRKY53* and/or *SAG201* expression, we generated *jmj16-1 wrky53* and
199 *jmj16-1 sag201* double mutants by genetically crossing *jmj16-1* with the
200 delayed-senescence mutants, *wrky53* and *sag201*. Evaluation of age-triggered leaf
201 senescence in the wild type, double mutants, and the corresponding parental lines
202 indicated that both the *wrky53* and *sag201* mutations partially suppressed the
203 early-senescence phenotype of *jmj16-1* (Figure 5). Taken together, these results
204 indicate that JMJ16 regulates leaf senescence at least partly through regulating
205 *WRKY53* and *SAG201* expression.

206 **Histone demethylase activity and specific domains of JMJ16 are required for the**
207 **regulation of leaf senescence**

208 The fruit fly (*Drosophila melanogaster*) H3K4me3 demethylase, Lid, regulates
209 developmental processes independently of its demethylase activity (Li et al., 2010).
210 To determine whether the histone demethylase activity of JMJ16 is involved in the
211 regulation of leaf senescence, we expressed constructs containing *JMJ16-HA* or
212 *JMJ16m-HA* driven by the *JMJ16* promoter in *jmj16-1* plants (Supplemental Figure

6A to 6C). Although both JMJ16-HA and JMJ16m-HA were directly associated with the chromatin region of *WRKY53* (Figure 3D), the expression of JMJ16-HA, but not JMJ16m-HA, rescued the early-senescence phenotype of *jmj16-1* and restored the transcription and H3K4me3 of *WRKY53* to wild type levels (Figure 3A to 3C), indicating that the early-senescence phenotype of this mutant is associated with the impaired histone demethylase activity of JMJ16.

JMJ16 contains five distinct domains, including the JmjN, JmjC, C5HC2 zinc finger (zf-C5HC2), F/Y-rich N-terminus (FYRN), and F/Y-rich C-terminal (FYRC) domains (Lu et al., 2008). To determine which domains are required for JMJ16 function, we generated four *JMJ16* mutant constructs harboring internal deletions of the JmjN, JmjC, or zf-C5HC2 domains or both the FYRN and FYRC (FYRN/C) domains driven by the *JMJ16* promoter (Supplemental Figure 6A). Like *jmj16* plants, transgenic *jmj16-1* plants expressing JmjN (Figure 3A to 3C; Supplemental Figure 6D and 6E), JmjC (Figure 3A to 3C; Supplemental Figure 6F and 6G), or FYRN/C (Figure 3A to 3C; Supplemental Figure 6J and 6K) internal deletion mutants of JMJ16 (referred to as *JMJ16ΔJN-HA*, *JMJ16ΔJC-HA*, and *JMJ16ΔFYR-HA*, respectively) exhibited an early-senescence phenotype, and the transcript and H3K4me3 levels of *WRKY53* were higher than those of wild type. By contrast, the expression of a JMJ16 deletion mutant lacking the zf-C5HC2 domain (referred to as *JMJ16ΔZF-HA*) rescued the early-senescence phenotype of *jmj16-1* and repressed the upregulated transcription and H3K4me3 levels of *WRKY53* in the *jmj16-1* genetic background (Figure 3A to 3C; Supplemental Figure 6H and 6I). These results indicate that the JmjN, JmjC, FYRN, and FYRC domains, but not the zf-C5HC2 domain, are required for the role of JMJ16 in the regulation of leaf senescence. We then investigated which domains of JMJ16 are required for its association with *WRKY53*. ChIP-qPCR analysis indicated that the JmjC and FYR domains are essential for the association of JMJ16 with *WRKY53*, but the JmjN and zf-C5HC2 domains are not (Figure 3D).

Age-dependent down-regulation of JMJ16 may be responsible for the activation

of SAG expression during senescence

To further elucidate the role of JMJ16 in regulating chromatin modifications of SAGs during leaf senescence, we determined the transcript levels, protein abundance and chromatin association of JMJ16 with SAGs during different developmental stages. *JMJ16* transcript levels slightly increased in wild-type plants during the aging process (Figure 6A and 6B). We examined JMJ16 protein levels in *JMJ16-HA* transgenic plants (*JMJ16-HA* driven by the *JMJ16* promoter expressed in the *jmj16-1* background). Immunoblot analysis using anti-HA antibody revealed that JMJ16-HA protein levels were slightly lower in the leaves of 5-week-old plants compared to 4-week-old plants but were substantially lower in the leaves of 6.5-week-old plants (Figure 6C). In contrast to the reduced JMJ16 levels, the levels of JMJ16 at *WRKY53* and *SAG201* were slightly higher in the leaves of 5- and 6.5-week-old plants compared to 4-week-old plants (Figure 6D).

Next, we monitored the transcript and H3K4me3 levels of *WRKY53* and *SAG201* at three developmental stages. In the leaves of 4-week-old wild-type and *jmj16-1* plants, *WRKY53* and *SAG201* transcripts were barely detectable, although basal levels of H3K4me3 modification were present at these loci (Figure 6E and 6F). These results suggest that JMJ16 does not affect the transcription or H3K4me3 levels of the SAGs at this stage, because if JMJ16 has an impact, H3K4me3 and the transcript levels of the SAGs would be higher in *jmj16-1*. However, in the leaves of 5-week-old plants, the transcript and H3K4me3 levels of these SAGs were substantially higher *jmj16-1* plants, but not in the wild type (Figure 6E and 6F), although no visible yellowing of leaves was observed in either line, suggesting that JMJ16 was able to affect gene expression and that the transition to senescence had begun in *jmj16-1* at this stage. In the leaves of 6.5-week-old wild-type plants, the transcript and H3K4me3 levels of the SAGs significantly increased (Figure 6E and 6F), along with a substantial reduction in the level of JMJ16 (Figure 6C). Taken together, these results suggest that the decreasing abundance of JMJ16 protein during the aging process may

be responsible for the increased H3K4me3 status and transcript levels of SAGs and the subsequent activation of leaf senescence.

DISCUSSION

The dynamic changes in H3K4me3 levels during leaf senescence may be regulated by H3K4me3 methyltransferases and/or demethylases; however, the enzymes that catalyze these changes have been elusive (Yolcu et al., 2018; Kim et al., 2018). We identified a JmjC domain-containing protein, JMJ16, which specifically demethylates H3K4me in Arabidopsis (Figure 2; Supplemental Figure 4). Loss-of-function *jmj16* mutants exhibited an early-senescence phenotype, which was rescued by complementation with JMJ16 (Figure 1). The conserved iron-binding amino acids in the JmjC domain of JMJ16 are required for its enzymatic activity and its regulation of leaf senescence (Figure 2B and 2C, and Figure 3A to 3C). RNA-seq and ChIP-seq analyses revealed that many SAGs are regulated by JMJ16 during leaf senescence through alterations of their associated H3K4me3 levels (Figure 4; Supplemental Figure 7). JMJ16 directly associates with the chromatin regions of *WRKY53* and *SAG201* and prevents precocious up-regulation of the transcription and H3K4me3 levels of these genes to maintain proper leaf aging. This finding is supported by the genetic evidence that the *wrky53* and *sag201* mutations suppress the early-senescence phenotype of *jmj16* (Figure 4J and 4N, and Figure 5).

In general, a histone demethylase is targeted to its target sites through its own DNA-binding domain or those of its partner proteins. For example, the H3K27 demethylase, RELATIVE OF EARLY FLOWERING6 (REF6), targets specific sites through its four tandem arrays of C2H2 zinc-finger domains, which directly bind to the CTCTGYTY motifs (Y=C/T) in its targets (Cui et al., 2016; Wang et al., 2018). The H3K4 demethylase, JMJ14, directly interacts with NAC domain-containing transcription factors through its FYRN/C domains, and the NAC transcription factors are required for the recruitment of JMJ14 to its specific target sites (Zhang et al.,

297 2015). The factors that determine the target specificity of JMJ16 are currently
298 unknown. JMJ16 contains JmjN, JmjC, zf-C5HC2, and FYRN/C domains (Lu et al.,
299 2008). Studies in budding yeast (*Saccharomyces cerevisiae*) revealed that the JmjN
300 domain is essential for the catalytic activity and protein stability of JmjC (Quan et al.,
301 2011; Chang et al., 2011; Klose et al., 2007; Liang et al., 2013). Expression of a
302 JMJ16 mutant protein lacking the JmjN domain did not rescue the early
303 senescence-related phenotypes of *jmj16*, but it did not affect its association with
304 *WRKY53*, suggesting that the JmjN domain is critical for the catalytic activity of
305 JMJ16 but does not affect its association with chromatin (Figure 3). In budding yeast
306 and mammals, the zf-C5HC2 domain of JmjC proteins is thought to be involved in
307 DNA binding and is required for the protein's function (Li et al., 2010; Liang et al.,
308 2013). Strikingly, however, in JMJ16, the zf-C5HC2 domain is dispensable for its
309 role in regulating leaf senescence and its association with chromatin (Figure 3),
310 suggesting that other domain(s) of JMJ16 might be involved in its association with
311 chromatin, such as the FYRN/C domains, since JMJ16 lacking FYRN/C domains
312 could not associates with its targets and was subsequently not be able to rescue the
313 early-senescence phenotype of *jmj16* (Figure 3). Similar to JMJ14, the FYRN/C
314 domains of JMJ16 may interacts with transcription factors, which recruit this protein
315 to its specific target sites. The identification of JMJ16-interacting proteins should help
316 us decipher the detailed mechanism underlying how JMJ16 is recruited to specific
317 chromatin target sites and regulates the H3K4 methylation status of
318 senescence-associated genes.

319 In animals, the histone H3K9 methyltransferase, G9a, stabilizes the association of
320 both H3K4 methyltransferase (MLL2/KMT2D) and H3K4 demethylase
321 (Jarid1a/KDM5A) at transcriptionally repressive target genes, where Jarid1a/KDM5A
322 removes the MLL2/KMT2D-mediated active mark H3K4me3 (Chaturvedi et al.,
323 2012). The detailed examination of H3K4me3 levels at the *WRKY53* and *SAG201* loci
324 during leaf senescence performed in the current study suggested that H3K4me3

modification is regulated by both H3K4me3 methylation and demethylation processes (Figure 6). The H3K4me3 levels of SAGs in 4-week-old wild-type and *jmj16* leaves were similar (Figure 6F), suggesting that H3K4me3 levels are tightly controlled during this developmental stage in both the wild type and *jmj16* mutant. In the leaves of 5-week-old (mature stage) JMJ16-HA complementation lines, the levels of association of *WRKY53* and *SAG201* with JMJ16 were slightly higher than those of the wild type (Figure 6D), but the H3K4me3 levels of the SAGs were not reduced in the wild type (Figure 6F). In *jmj16-1*, however, H3K4me3 levels at these loci were substantially up-regulated at the mature stage (Figure 6F), suggesting that H3K4 methylation activity may also be required to maintain balance between H3K4me3 methylation/demethylation status at the mature stage. In the leaves of 6.5-week-old JMJ16-HA complementation lines, JMJ16 protein levels were substantially reduced (Figure 6C), and H3K4me3 levels at *WRKY53* and *SAG201* were increased in the wild type (Figure 6F), suggesting that the balance of H3K4me3 methylation/demethylation started to shift towards methylation in the wild type. Taken together, these findings suggest that the age-dependent increase in H3K4 levels of SAGs is regulated by both H3K4 methyltransferase(s) and JMJ16 in Arabidopsis and that the gradually decreasing levels of JMJ16 during leaf aging may contribute to the up-regulation of H3K4me3 levels observed for the SAGs. Although the detailed mechanisms are unknown, H3K4me3 methylation/demethylation are thought to be involved in regulating aging in mammals (Greer et al., 2010). Thus, H3K4me3 methyltransferase/demethylase may have conserved functions in the regulation of aging in both plants and mammals.

METHODS

Plant materials and growth conditions

All *Arabidopsis thaliana* lines used in this study were in the Col-0 background. The *jmj16-1* (SAIL_535_F09), *jmj16-2* (SAIL_80_F06), *jmj16-3* (SALK_029530),

353 *jmj17-1* (SALK_014109), *jmj17-2* (SALK_037362), and *sag201* (SALK_142329)
354 lines were obtained from the Nottingham Arabidopsis Stock Centre. The *jmj14-1*
355 (SALK_135712) and *jmj18-1* (SALK_073422) were described previously (Lu et al.,
356 2010; Yang et al., 2012a). The *wrky53* mutant (SALK_034157) was a gift from Dr.
357 Ulrike Zentgraf (Department of General Genetics, University of Tuebingen) and has
358 been described in a previous report (Miao and Zentgraf, 2007). The *wrky53 jmj16* and
359 *sag201 jmj16* double mutants were generated by genetic crossing of *jmj16-1* with
360 *wrky53* and *sag201*, respectively. The primers used for genotyping are listed in
361 Supplemental Data Set 6. Surface-sterilized seeds were imbibed for 3 d at 4°C to
362 break seed dormancy. The stratified seeds were grown on MS plates for 6 days, and
363 the seedlings were transferred to soil. All plants were grown in a culture room at 22°C
364 under a 16-h-light (approximately 100 μmol m^{-2} sec^{-1}; five 6500 K T5 fluorescent
365 lamps plus one 2700 K T5 fluorescent lamp)/8-h-dark cycle.

366 **Analysis of leaf senescence phenotypes**

367 Rosette leaves of plants at the indicated developmental stages were detached and
368 photographed. The mature stage and early senescence (ES) stages mentioned in this
369 article were defined based on previous work, with minor modifications (van der
370 Graaff et al., 2006). Briefly, mature stage leaves indicate fully expanded leaves 5 and
371 6 of plants without a visible yellowing phenotype. Early senescence leaves represent
372 leaves 5 and 6 of plants with an approximately 10-25% tip-yellowing phenotype. The
373 chlorophyll content analysis method has been described previously (Porra et al., 1989).
374 The *Fv/Fm* ratio was determined using a PAM 2000 portable chlorophyll fluorometer
375 connected by a leaf-clip holder with a trifurcated fiber optic cable (Heinz Walz,
376 Germany) based on previous work (Cai et al., 2010).

377 **Plasmid construction**

378 To generate pCambia1303-ProJMJ16:JMJ16, a fragment containing a 2.0-kb
379 promoter region and 3.2-kb genomic fragment of *JMJ16* was amplified with primer
380 pairs MiniPro and genomic1-F SalI/ MiniPro and genomic1-R NcoI and cloned into

the pBluescript vector to generate pBluescript-JMJ16P/G1. pBluescript-JMJ16P/G1 was digested with *Sal*I/*Nco*I and inserted into the *Sal*I/*Nco*I sites of the pCambia1303 vector to generate pCambia1303-JMJ16P/G1. The remaining genomic fragment of JMJ16 was amplified with the No-genomic2 F/No-genomic2-R primer pair and digested with *Nco*I to generate a 5'-sticky/3'-blunt end insert (JMJ16G2). pCambia1303-JMJ16P/G1 was digested with *BstE*II, blunted with Mung bean enzyme, and digested with *Nco*I. The digested JMJ16G2 insert was ligated into the pCambia1303-JMJ16P/G1 vector to generate pCambia1303-ProJMJ16:JMJ16.

To generate pCambia1300-ProJMJ16:JMJ16ΔJN-HA, pCambia1300-ProJMJ16:JMJ16ΔJC-HA, pCambia1300-ProJMJ16:JMJ16ΔZF-HA, and pCambia1300-ProJMJ16:JMJ16ΔFYR-HA, a genomic DNA fragment containing the promoter and coding region of *JMJ16* was amplified with the J16 Promoter XmaI F/J16 No stop SalI R primer pair, and ligated into the pBluescript vector to generate pBluescript-JMJ16P/G. Fragments containing each internal deletion were generated using specific primers listed in Supplemental Data Set 6, and the wild-type *JMJ16* genomic sequence in pBluescript-JMJ16P/G was replaced with each of these fragments. These pBluescript-*JMJ16* deletion constructs were digested with *Xma*I/*Sal*I and ligated into the *Xma*I/*Sal*I sites of the modified pCambia1300-HA vector.

To construct pCambia1300-ProJMJ16:JMJ16-HA (XF2090), approximately 0.8 kb of the 3'UTR of *JMJ16* was cloned using the CX9288 and CX9289 primers and introduced into pCambia1300-HA after *Nco*I digestion. The full-length genomic region and native promoter of *JMJ16* were then amplified using the CX9286 and CX9287 primers and inserted into pCambia1300-HA-UTR by *Xma*I and *Pst*I digestion. pJMJ16:JMJ16m-HA (XF2091) was generated by site-directed mutagenesis using a QuickChange Kit (Stratagene) with the HX2343 and HX2344 primers.

To construct pEG101-Pro35S:JMJ16-YFP-HA (XF2177), the full-length

genomic coding region of *JMJ16* was amplified using the CX3619 and CX3620 primers, cloned into pENTR/D-TOPO (Invitrogen), and introduced by the LR reaction into the pEarleyGate101 (pEG101) vector with a C-terminal YFP-HA tag. pEG101-Pro35S:JMJ16m-YFP-HA (XF2178) was generated by site-directed mutagenesis using a QuickChange Kit (Stratagene) with the HX2343 and HX2344 primers.

To construct pGEX-5X-1-JMJ14$_{596}$, a 1,788 bp cDNA fragment of *JMJ14* was amplified with primer pairs J14 (596) SalI F and J14 (596) NotI R. The PCR product was digested with *Sal*I/*Not*I and inserted into the *Sal*I/*Not*I sites of the pGEX-5X-3 vector to generate pGEX-5X-3-JMJ14$_{596}$.

To construct pGEX-5X-1-JMJ16$_{670}$, a 2,010 bp cDNA fragment of *JMJ16* was amplified with primer pairs J16 (670) XbaI F and J16 (670) SalI R. The PCR product was digested with *Xba*I/*Sal*I and inserted into the *Xba*I/*Sal*I sites of the pGEX-5X-1-Myc vector to generate pGEX-5X-1-JMJ16$_{670}$.

Transgenic plant generation

The pCambia1303-ProJMJ16:JMJ16, pCambia1300-ProJMJ16:JMJ16-HA, pCambia1300-ProJMJ16:JMJ16m-HA, pCambia1300-ProJMJ16:JMJ16ΔJN-HA, pCambia1300-ProJMJ16:JMJ16ΔJC-HA, pCambia1300-ProJMJ16:JMJ16ΔZF-HA, and pCambia1300-ProJMJ16:JMJ16ΔFYR-HA constructs were transformed into *Agrobacterium tumefaciens* cells (strain GV3101) and then stably transformed into *jmj16-1* mutant plants using the floral dip method (Clough and Bent, 1998). pEG101-Pro35S:JMJ16-YFP-HA was stably transformed into Arabidopsis wild-type Col-0 as described above.

In vivo histone demethylation assay

The procedures used for the in vivo histone demethylation assay were described previously (Lu et al., 2011). Briefly, pEG101-Pro35S:JMJ16-YFP-HA and pEG101-Pro35S:JMJ16m-YFP-HA constructs were transformed into *Agrobacterium tumefaciens* cells (strain EHA105), and the cells were then infiltrated into *Nicotiana*

benthamiana leaves. To determine the specific histone methylation status, immunostaining was performed using histone methylation-specific antibodies (H3K4me3: Millipore 07-473, 1:100; H3K4me2: Millipore 07-030, 1:500; H3K4me1: Millipore 07-436, 1:100; H3K9me3: Millipore 07-442, 1:100; H3K9me2: Millipore 07-441, 1:200; H3K9me1: Millipore 07-450, 1:100; H3K27me3: Millipore 07-449, 1:100; H3K27me2: Millipore 07-452, 1:100; H3K27me1: Millipore 07-448, 1:100; H3K36me3: Abcam ab9050, 1:100; H3K36me2: Millipore 07-274, 1:100; and H3K36me1: Millipore 07-548, 1:100) and Alexa Fluor 488-conjugated goat anti-rabbit (1:200, Invitrogen). The YFP and Alexa Fluor 488 fluorescent signals were photographed under a fluorescence microscope (Olympus BX51). ImageJ (National Institutes of Health) software was used to quantify the fluorescent signals in immunolabeled nuclei as described previously (Lu et al., 2011).

In vitro histone demethylation assay

An in vitro demethylation assay was performed as previously described, with minor modifications (Yang et al., 2010). Briefly, GST-JMJ14$_{596}$, GST-JMJ16$_{670}$ and GST proteins were expressed in *E. coli* and affinity purified with Glutathione Sepharose 4B resin (GE Healthcare). 4.0 μg of calf thymus histones (Sigma H9250) were incubated with affinity-purified GST-JMJ14$_{596}$ (1 μg), GST-JMJ16$_{670}$ (2 μg) or GST (5 μg) in 40 μl reaction buffer (20 mM Tris-Cl pH 7.5, 150 mM NaCl, 50 μM $Fe(NH_4)_2(SO_4)_2$, 1 mM α-ketoglutarate, 2 mM ascorbate) for 5 h at 37°C. The reaction product was analyzed by protein gel blot analysis with anti-H3K4me3 (Abcam ab8580), anti-H3K4me2 (Millipore 07-030), anti-H3K4me1 (Millipore 07-436), H3K9me2 (Millipore 07-441), H3K9me1 (Millipore 07-450), H3K27me3 (Millipore 07-449), H3K27me2 (Millipore 07-452), H3K27me1 (Millipore 07-448), H3K36me3 (Abcam ab9050), H3K36me2 (Millipore 07-274), H3K36me1 (Millipore 07-548) and anti-H3 (Abcam ab1791).

RNA extraction and RT-qPCR analysis

Total RNA was extracted from seedlings and rosette leaves with TRIZOL (RNAiso

Plus TaKaRa) and reverse transcribed with a Revert Aid First Strand cDNA Synthesis Kit (Thermo Scientific). RT-qPCR analysis was performed on a MP3000 instrument (Stratagene) with SYBR Premix ExTaq (TaKaRa), 40 cycles were used for all qPCR analyses. Primer sequences for RT-qPCR analysis are listed in Supplemental Data Set 6.

Chromatin immunoprecipitation assay (ChIP) and library preparation

ChIP was performed as described previously with minor modifications (Lu et al., 2011). Briefly, 1 g of tissue from leaves 5 and 6 at the indicated developmental stages from Col-0, *jmj16-1* and transgenic *jmj16-1* plants expressing full-length JMJ16, JMJ16m, JmjN, JmjC, zf-C5HC2 or FYRN/C internal deletion mutants driven by its own promoter were harvested, ground in liquid nitrogen, and cross-linked with formaldehyde. Anti-HA (Sigma H6908), anti-H3K4me3 (Millipore 07-473) and anti-H3 (Abcam ab1791) were used for immunoprecipitation as described previously (Zhang et al., 2015). Immunoprecipitated DNA was used for ChIP-seq DNA library preparation or qPCR analysis. A ChIP-seq library was constructed using the NEBNext® DNA Library Prep Master Mix Set for Illumina® (NEB, E6040S).

ChIP-seq and RNA-seq analysis

ChIP-seq reads were aligned to the *Arabidopsis thaliana* genome (TAIR10 release) using Bowtie 2 (Langmead and Salzberg, 2012) with default parameters and the local alignment model. Duplicated reads and low mapping quality reads (MAQ<30) were identified and removed using Samtools (Li et al., 2009). Enriched intervals were identified using MACS (Zhang et al., 2008) with default parameters. Density maps of reads for visualization were based on counts of the 200-bp extension of sequencing reads in the 3' direction (as described in Ernst et al., 2011) followed by RPGC (Reads Per Genomic Content) normalization. Hypermethylation of H3K4me3 between the *jmj16* mutant and wild type were detected using the ChIPDiff program with a 1.5-fold change as described previously (Lu et al., 2011). Significantly enriched regions of JMJ16 were identified based on 2-fold change comparing to the *jmj16-1* genetic

493 background. RNA-seq reads were firstly aligned to the *Arabidopsis thaliana*
494 transcriptome (based on the TAIR10 annotation) using TopHat 2 (Kim et al., 2013)
495 with default parameters for further visualization in IGB (Integrated Genome Browser
496 from BioViz) with ChIP-seq data. Meanwhile, RNA-seq reads were remapped and
497 quantitatively evaluated using Salmon (Patro et al., 2017). Differentially expressed
498 genes between the *jmj16-1* mutant and wild type were identified using 1.5-fold
499 change as the cut-off. Meta-gene analysis and heatmap plotting were performed using
500 deepTools (Ramírez et al., 2016).

501 **Statistical analysis**

502 Data were analyzed by Student's *t*-test or one-way ANOVA with Tukey's honestly
503 significant difference test (Supplemental Data Set 7).

504 **Accession Numbers**

505 Sequence data from this study can be found in the Arabidopsis Genome Initiative
506 database under the following accession numbers: *CRK36* (At4g04490), *eIF4a*
507 (At3g13920), *JMJ14* (At4g20400), *JMJ16* (At1g08620), *JMJ17* (At1g63490), *JMJ18*
508 (At1g30810), *SAG12* (At5g45890), *SAG13* (At2g29350), *SAG201* (At2g45210),
509 *UBC21* (At5g25760), *WRKY53* (At4g23810). RNA-seq and ChIP-seq data from this
510 article can be found in the Gene Expression Omnibus data library under accession
511 number GSE115362.

512 **Supplemental Data**

513 **Supplemental Figure 1.** Characterization of *jmj16* T-DNA insertion mutants.

514 **Supplemental Figure 2.** Mutation in *JMJ16*, but not *JMJ14*, *JMJ17* or *JMJ18*, causes
515 early senescence phenotype.

516 **Supplemental Figure 3.** Additional examples of *JMJ16* complementation transgenic
517 plants.

518 **Supplemental Figure 4.** JMJ16 does not exhibit H3K9, H3K27, or H3K36
519 demethylase activity *in vivo* or *in vitro*.

Supplemental Figure 5. JMJ16 expression levels in *JMJ16 OE* transgenic plants.

Supplemental Figure 6. Characterization of transgenic plants expressing JMJ16 mutant proteins.

Supplemental Figure 7. Transcript and H3K4me3 methylation levels of JMJ16-HA associated genes are up-regulated in *jmj16-1*.

Supplemental Data Set 1. Differentially expressed genes in *jmj16-1*.

Supplemental Data Set 2. JMJ16 target genes.

Supplemental Data Set 3. Hypermethylation of H3K4me3 in *jmj16-1*.

Supplemental Data Set 4. JMJ16 target genes with upregulated expression and hyperH3K4me3 in *jmj16-1*.

Supplemental Data Set 5. LSD 2.0 genes with JMJ16 binding and hyperH3K4me3 in *jmj16-1*.

Supplemental Data Set 6. Primers used in this study.

Supplemental Data Set 7. Parameters used for ANOVA statistical analyses.

ACKNOWLEDGMENTS

We thank Dr. Ulrike Zentgraf for the *wrky53* (SALK_034157) seeds. This work was supported by National Natural Science Foundation of China Grants (31788103, 91540203 to X. Cao, 31471363 to J.B. Jin), Key Research Program of Frontier Sciences Chinese Academy of Sciences (Grant No. QYZDY-SSW-SMC022 to X. Cao), and Chinese Academy of Sciences (The Innovative Academy of Seed Design to X. Cao and J.B. Jin).

AUTHOR CONTRIBUTIONS

P.L., S.Z., X.C., and J.B.J. designed the study. P.L., S.Z., X.L., X.F.Z., B.C., Y.H.J., and N.D. performed the research. P.L., S.Z., B.Z., X.C., J.L., and J.B.J. analyzed the data. P.L., S.Z., B.Z., X.C., and J.B.J. wrote the paper.

REFERENCES

Ay, N., Irmler, K., Fischer, A., Uhlemann, R., Reuter, G., and Humbeck, K. (2009). Epigenetic programming via histone methylation at WRKY53 controls leaf senescence in *Arabidopsis thaliana*. Plant J. **58**: 333-346.

Balazadeh, S., Riaño-Pachón, D.M., and Mueller-Roeber B. (2008). Transcription factors regulating leaf senescence in *Arabidopsis thaliana*. Plant Biol. (Stuttg) **10** (Suppl 1): 63-75.

Brusslan, J.A., Rus Alvarez-Canterbury, A.M., Nair, N.U., Rice, J.C., Hitchler, M.J., and Pellegrini, M. (2012). Genome-wide evaluation of histone methylation changes associated with leaf senescence in Arabidopsis. PLoS One **7**: e33151.

Cai, B., Zhang, A., Yang, Z., Lu, Q., Wen, X., and Lu, C. (2010). Characterization of photosystem II photochemistry in transgenic tobacco plants with lowered Rubisco activase content. J. Plant Physiol. **167**: 1457-1465.

Chang, Y., Wu, J., Tong, X.J., Zhou, J.Q., and Ding, J. (2011). Crystal structure of the catalytic core of *Saccharomyces cerevesiae* histone demethylase Rph1: insights into the substrate specificity and catalytic mechanism. Biochem. J. **433**: 295-302.

Chaturvedi, C.P., Somasundaram, B., Singh, K., Carpenedo, R.L., Stanford, W.L., Dilworth, F.J., and Brand, M. (2012). Maintenance of gene silencing by the coordinate action of the H3K9 methyltransferase G9a/KMT1C and the H3K4 demethylase Jarid1a/KDM5A. Proc. Natl. Acad. Sci. USA. **109**: 18845-18850.

Clough, S.J., and Bent, A.F. (1998). Floral dip: a simplified method for Agrobacterium-mediated transformation of *Arabidopsis thaliana*. Plant J. **16**: 735-743.

Cui, X., Lu, F., Qiu, Q., Zhou, B., Gu, L., Zhang, S., Kang, Y., Cui, X., Ma, X., Yao, Q., Ma, J., Zhang, X., and Cao, X. (2016). REF6 recognizes a specific DNA sequence to demethylate H3K27me3 and regulate organ boundary formation in Arabidopsis. Nat. Genet. **48**: 694-699.

Ernst, J., Kheradpour, P., Mikkelsen, T.S., Shoresh, N., Ward, L.D., Epstein, C.B., Zhang X, Wang L, Issner, R., Coyne, M., Ku, M., Durham, T., Kellis, M.,

and Bernstein, B.E. (2011). Mapping and analysis of chromatin state dynamics in nine human cell types. Nature **473**: 43-49.

Greer, E.L., Maures, T.J., Hauswirth, A.G., Green, E.M., Leeman, D.S., Maro, G.S., Han, S., Banko, M.R., Gozani, O., and Brunet, A. (2010). Members of the H3K4 trimethylation complex regulate lifespan in a germline-dependent manner in *C. elegans*. Nature **466**: 383-387.

Hou, K., Wu, W., and Gan, S.S. (2013). SAUR36, a small auxin up RNA gene, is involved in the promotion of leaf senescence in Arabidopsis. Plant Physiol. **161**: 1002-1009.

Huang, D., Lan, W., Li, D., Deng, B., Lin, W., Ren, Y., and Miao, Y. (2018). WHIRLY1 occupancy affects histone lysine modification and *WRKY53* transcription in Arabidopsis developmental manner. Front. Plant Sci. **9**: 1503.

Jing, Y., Sun, H., Yuan, W., Wang, Y., Li, Q., Liu Y, Li, Y., and Qian, W. (2016). SUVH2 and SUVH9 couple two essential steps for transcriptional gene silencing in Arabidopsis. Mol. Plant **9**:1156-1167.

Kim, D., Pertea, G., Trapnell, C., Pimentel, H., Kelley, R., and Salzberg, S.L. (2013). TopHat2: accurate alignment of transcriptomes in the presence of insertions, deletions and gene fusions. Genome Biol. **14**: R36.

Kim, J., Kim, J.H., Lyu, J.I., Woo, H.R., and Lim, P.O. (2018). New insights into the regulation of leaf senescence in Arabidopsis. J. Exp. Bot. **69**: 787-799.

Kim, J.H., Woo, H.R., Kim, J., Lim, P.O., Lee, I.C., Choi, S.H., Hwang, D., and Nam, H.G. (2009). Trifurcate feed-forward regulation of age-dependent cell death involving miR164 in Arabidopsis. Science **323**: 1053-1057.

Klose, R.J., Gardner, K.E., Liang, G., Erdjument-Bromage, H., Tempst, P., and Zhang, Y. (2007). Demethylation of histone H3K36 and H3K9 by Rph1: a vestige of an H3K9 methylation system in *Saccharomyces cerevisiae*? Mol. Cell Biol. **27**: 3951-3961.

Langmead, B., and Salzberg, S.L. (2012). Fast gapped-read alignment with Bowtie 2. Nat. Methods **9**: 357-359.

Li, H., Handsaker, B., Wysoker, A., Fennell, T., Ruan, J., Homer, N., Marth, G., Abecasis, G., and Durbin, R. (2009). The sequence alignment/map format and SAMtools. Bioinformatics **25**: 2078-2079.

Li, L., Greer, C., Eisenman, R.N., and Secombe, J. (2010). Essential functions of the histone demethylase lid. PLoS Genet. **6**: e1001221.

Li, Z., Peng, J., Wen, X., and Guo, H. (2012). Gene network analysis and functional studies of senescence-associated genes reveal novel regulators of Arabidopsis leaf senescence. J. Integr. Plant Biol. **54**: 526-539.

Li, Z., Zhao, Y., Liu, X., Peng, J., Guo, H., and Luo, J. (2014). LSD 2.0: an update of the leaf senescence database. Nucleic Acids Res. **42**(Database issue): D1200-1205.

Liang, C.Y., Wang, L.C., and Lo, W.S. (2013). Dissociation of the H3K36 demethylase Rph1 from chromatin mediates derepression of environmental stress-response genes under genotoxic stress in *Saccharomyces cerevisiae*. Mol. Biol. Cell **24**: 3251-3262.

Lim, P.O., Kim, H.J., and Nam, H.G. (2007). Leaf senescence. Annu. Rev. Plant Biol. **58**: 115-136.

Liu, Z.W., Shao, C.R., Zhang, C.J., Zhou, J.X., Zhang, S.W., Li, L., Chen, S., Huang, H.W., Cai, T., and He, X.J. (2014). The SET domain proteins SUVH2 and SUVH9 are required for Pol V occupancy at RNA-directed DNA methylation loci. PLoS Genet. **10**: e1003948.

Lu, F., Cui, X., Zhang, S., Jenuwein, T., and Cao, X. (2011). Arabidopsis REF6 is a histone H3 lysine 27 demethylase. Nat. Genet. **43**: 715-719.

Lu, F., Cui, X., Zhang, S., Liu, C., and Cao, X. (2010). JMJ14 is an H3K4 demethylase regulating flowering time in Arabidopsis. Cell Res. **20**: 387-390.

Lu, F., Li, G., Cui, X., Liu, C., Wang, X.J., and Cao, X. (2008). Comparative analysis of JmjC domain-containing proteins reveals the potential histone demethylases in Arabidopsis and rice. J. Integr. Plant Biol. **50**: 886-896.

Miao, Y., Laun, T., Zimmermann, P., and Zentgraf, U. (2004). Targets of the WRKY53 transcription factor and its role during leaf senescence in Arabidopsis. Plant Mol. Biol. **55**: 853-867.

Miao, Y., Jiang, J., Ren, Y., and Zhao, Z. (2013). The single-stranded DNA-binding protein WHIRLY1 represses *WRKY53* expression and delays leaf senescence in a developmental stage-dependent manner in Arabidopsis. Plant Physiol. **163**: 746-756.

Miao, Y., and Zentgraf, U. (2007). The antagonist function of Arabidopsis WRKY53 and ESR/ESP in leaf senescence is modulated by the jasmonic and salicylic acid equilibrium. Plant Cell **19**: 819-830.

Oh, S.A., Lee, S.Y., Chung, I.K., Lee, C.H., and Nam, H.G. (1996). A senescence-associated gene of *Arabidopsis thaliana* is distinctively regulated during natural and artificially induced leaf senescence. Plant Mol. Biol. **30**: 739-754.

Pan, R., Reumann, S., Lisik, P., Tietz, S., Olsen, L.J., Hu, J. (2018). Proteome analysis of peroxisomes from dark-treated senescent Arabidopsis leaves. J. Integr. Plant Biol. **60**: 1028-1050.

Patro, R., Duggal, G., Love, M.I., Irizarry, R.A., and Kingsford, C. (2017). Salmon provides fast and bias-aware quantification of transcript expression. Nat. Methods **14**: 417-419.

Porra, R.J., Thompson, W.A., and Kriedemann, P.E. (1989). Determination of accurate extinction coefficients and simultaneous equations for assaying chlorophylls *a* and *b* extracted with four different solvents: verification of the concentration of chlorophyll standards by atomic absorption spectroscopy. Biochim. Biophys. Acta **975**: 384-394.

Quan, Z., Oliver, S.G., and Zhang, N. (2011). JmjN interacts with JmjC to ensure selective proteolysis of Gis1 by the proteasome. Microbiology **157**: 2694-2701.

Ramírez, F., Ryan, D.P., Grüning, B., Bhardwaj, V., Kilpert, F., Richter, A.S., Heyne, S., Dündar, F., and Manke, T. (2016). deepTools2: A next generation web server for deep-sequencing data analysis. Nucleic Acids Res. **44**: W160-165.

Robatzek, S., and Somssich, I.E. (2002). Targets of AtWRKY6 regulation during plant senescence and pathogen defense. Genes Dev. **16**: 1139-1149.

van der Graaff, E., Schwacke, R., Schneider, A., Desimone, M., Flügge, U.I., and Kunze, R. (2006). Transcription analysis of Arabidopsis membrane transporters and hormone pathways during developmental and induced leaf senescence. Plant Physiol. **141**: 776-792.

Wang, X., Gao, J., Gao, S., Li, Z., Kuai, B., and Ren, G. (2018). REF6 promotes lateral root formation through de-repression of *PIN1*/*3*/*7* genes. J. Integr. Plant Biol. doi: 10.1111/jipb.12726.

Woo, H.R., Chung, K.M., Park, J.H., Oh, S.A., Ahn, T., Hong, S.H., Jang, S.K., and Nam, H.G. (2001). ORE9, an F-box protein that regulates leaf senescence in Arabidopsis. Plant Cell **13**: 1779-1790.

Woo, H.R., Kim, H.J., Nam, H.G., and Lim, P.O. (2013). Plant leaf senescence and death - regulation by multiple layers of control and implications for aging in general. J. Cell Sci. **126**: 4823-4833.

Xie, Y., Huhn, K., Brandt, R., Potschin, M., Bieker, S., Straub, D., Doll, J., Drechsler, T., Zentgraf, U., and Wenkel, S. (2014). REVOLUTA and WRKY53 connect early and late leaf development in Arabidopsis. Development **141**: 4772-4783.

Yang, H., Han, Z., Cao, Y., Fan, D., Li, H., Mo, H., Feng, Y., Liu, L., Wang, Z., Yue, Y., Cui, S., Chen, S., Chai, J., and Ma, L. (2012a). A companion cell-dominant and developmentally regulated H3K4 demethylase controls

685 flowering time in Arabidopsis via the repression of *FLC* expression. PLoS Genet. **8**:
686 e1002664.
687 **Yang, H., Mo, H., Fan, D., Cao, Y., Cui, S., and Ma, L.** (2012b). Overexpression of
688 a histone H3K4 demethylase, JMJ15, accelerates flowering time in Arabidopsis.
689 Plant Cell Rep. **31**: 1297-1308.
690 **Yang, W., Jiang, D., Jiang, J., and He, Y.** (2010). A plant-specific histone H3 lysine
691 4 demethylase represses the floral transition in Arabidopsis. Plant J. **62**: 663-673.
692 **Yolcu, S., Li, X., Li, S., and Kim, Y.J.** (2018). Beyond the genetic code in leaf
693 senescence. J. Exp. Bot. **69**: 801-810.
694 **Zhang, S., Zhou, B., Kang, Y., Cui, X., Liu, A., Deleris, A., Greenberg, M.V., Cui,**
695 **X., Qiu, Q., Lu, F., Wohlschlegel, J.A., Jacobsen, S.E., and Cao, X.** (2015).
696 C-terminal domains of histone demethylase JMJ14 interact with a pair of NAC
697 transcription factors to mediated specific chromatin association. Cell Discov. **1**:
698 15003.
699 **Zhang, X., Bernatavichute, Y.V., Cokus, S., Pellegrini, M., and Jacobsen, S.E.**
700 (2009). Genome-wide analysis of mono-, di- and trimethylation of histone H3
701 lysine 4 in *Arabidopsis thaliana*. Genome Biol. **10**: R62.
702 **Zhang, Y., Liu, T., Meyer, C.A., Eeckhoute, J., Johnson, D.S., Bernstein, B.E.,**
703 **Nusbaum, C., Myers, R.M., Brown, M., Li, W., and Liu, X.S.** (2008).
704 Model-based analysis of ChIP-Seq (MACS). Genome Biol. **9**: R137.
705 **Zhou, X., Jiang, Y., and Yu, D.** (2011). WRKY22 transcription factor mediates
706 dark-induced leaf senescence in Arabidopsis. Mol. Cells **31**: 303-313.

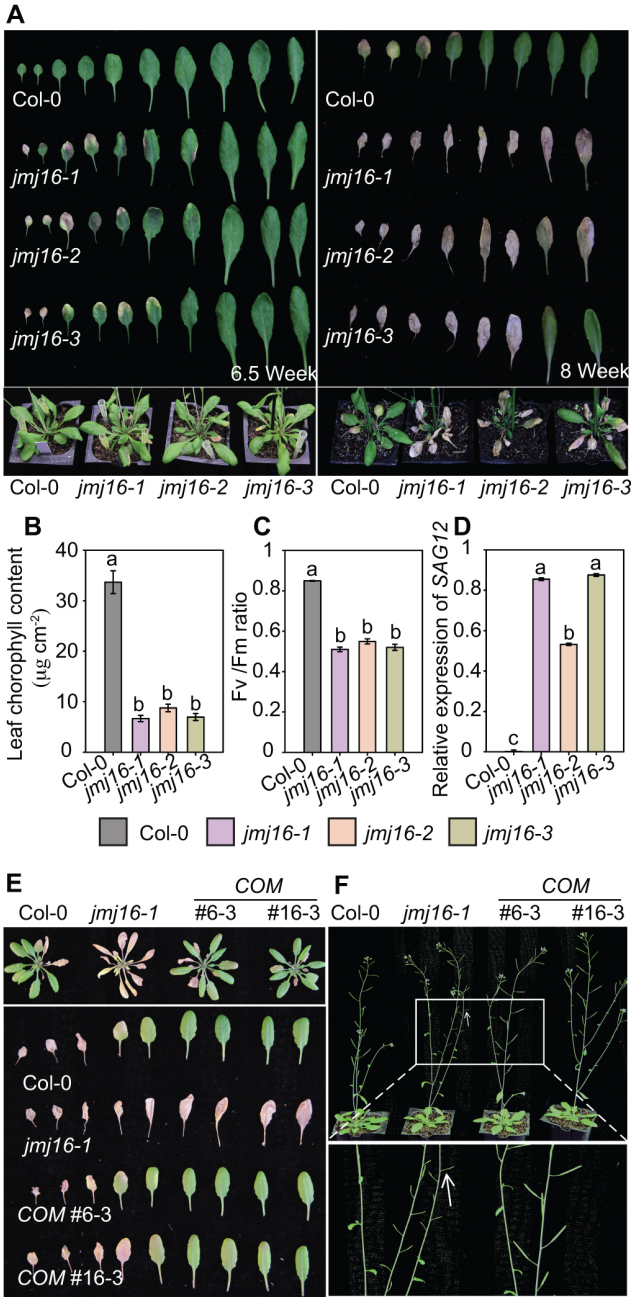

Figure 1. Leaf senescence phenotypes of *jmj16* T-DNA insertion mutants and complementation transgenic plants.
(A) Leaf senescence phenotypes. Plants were grown under long-day conditions for 6.5 weeks (left panel) or 8 weeks (right panel).
(B) to **(D)** Chlorophyll content **(B)**, Fv/Fm ratio **(C)**, and expression level of *SAG12* **(D)** in leaves 5 and 6 of 6.5-week-old plants. Relative expression was normalized to that of *eIF4a*. Error bars represent ± SD (n=3). Different letters indicate significant differences among genotypes based on one-way ANOVA with Tukey's honestly significant difference test ($P < 0.0001$).
(E) Leaf senescence phenotypes of 7-week-old wild-type, *jmj16,* and complementation plants.
(F) The *jmj16-1* mutant exhibits an aborted silique phenotype, which is rescued by the expression of JMJ16. Six-week-old plants were photographed; a magnified view of the area in the rectangle is shown in the bottom panel. Arrow indicates aborted silique. *COM* indicates the expression of *JMJ16* driven by its own promoter in *jmj16-1*.

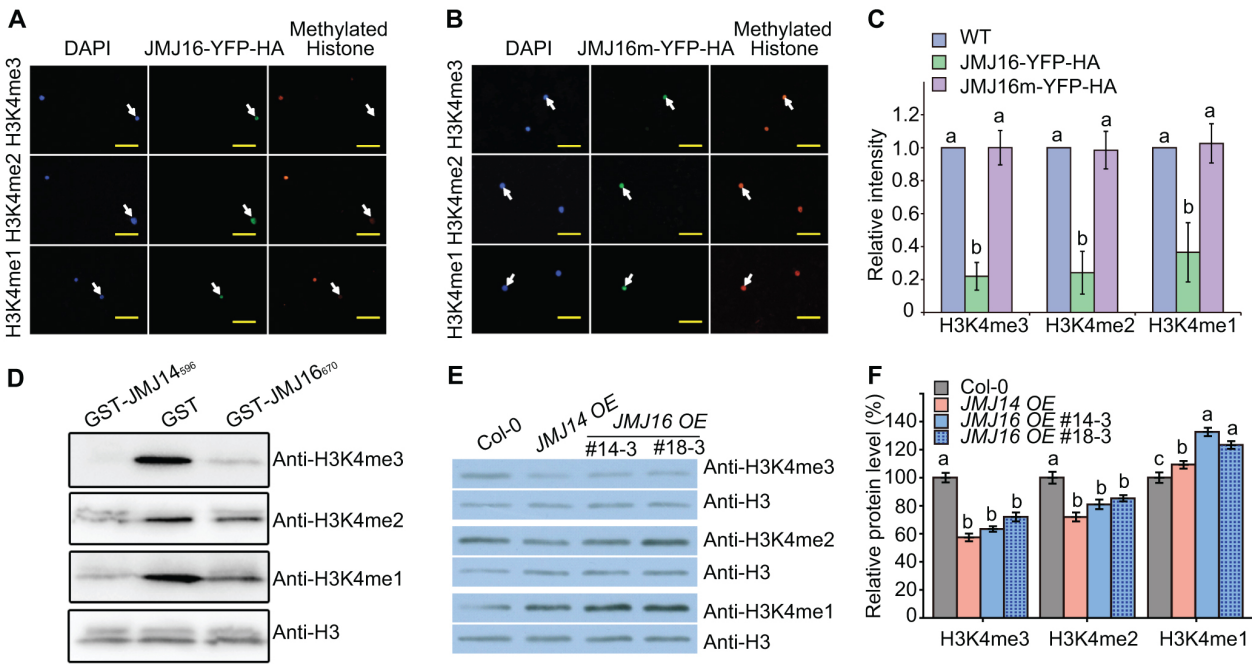

Figure 2. JMJ16 is an H3K4 demethylase.
(A) JMJ16-YFP-HA exhibits H3K4me1/2/3 demethylase activity in *Nicotiana benthamiana* leaves.
(B) Mutations in conserved Fe (II) binding amino acids (JMJ16m-YFP-HA) abolish its H3K4me1/2/3 demethylase activity in *Nicotiana benthamiana* leaves. In **(A)** and **(B)**, JMJ16-YFP-HA and JMJ16m-YFP-HA expression in *Nicotiana benthamiana* nuclei (arrows) was visualized by monitoring YFP fluorescence (green, middle panel). The histone methylation status was analyzed by immunostaining with specific histone methylation antibodies (red, right panel). The location of nuclei was visualized using DAPI staining (blue, left). Scale bars indicate 5 μm.
(C) Statistical analysis of the levels of fluorescent signals in **(A)** and **(B)**. At least 25 pairs of JMJ16-YFP-HA- or JMJ16m-YFP-HA-expressing versus non-expressing nuclei in the same field of view were analyzed. Error bars represent ± SD. Different letters indicate significant differences based on one-way ANOVA with Tukey's honestly significant difference test ($P < 0.01$).
(D) GST-JMJ16$_{670}$ exhibits H3K4me1/2/3 demethylase activity in vitro. *E. coli*-expressed and affinity purified GST-JMJ16$_{670}$ was incubated with calf thymus histone, and the H3K4 methylation status were determined using methylation-specific antibodies. GST-JMJ14$_{596}$ was used as a positive control and anti-H3 was used as a loading control.
(E) Global H3K4 methylation status of 10-day-old plants. *JMJ14 OE* and *JMJ16 OE* indicate the expression of *JMJ14-YFP-HA* and *JMJ16-YFP-HA* driven by the 35S promoter in Col-0, respectively. Methylation-specific antibodies were used to determine the global H3K4 methylation status. Anti-H3 was used as a loading control.
(F) Quantification analysis of **(E)**. Immunoblots of three biological replicates were quantified, each replicate means that immunoblots were performed using freshly prepared protein extracts from Col-0, *JMJ14-OE* and *JMJ16 OE* (#14-3 and #18-3). Error bars represent ± SD. Different letters indicate significant differences among genotypes based on one-way ANOVA with Tukey's honestly significant difference test ($P < 0.05$).

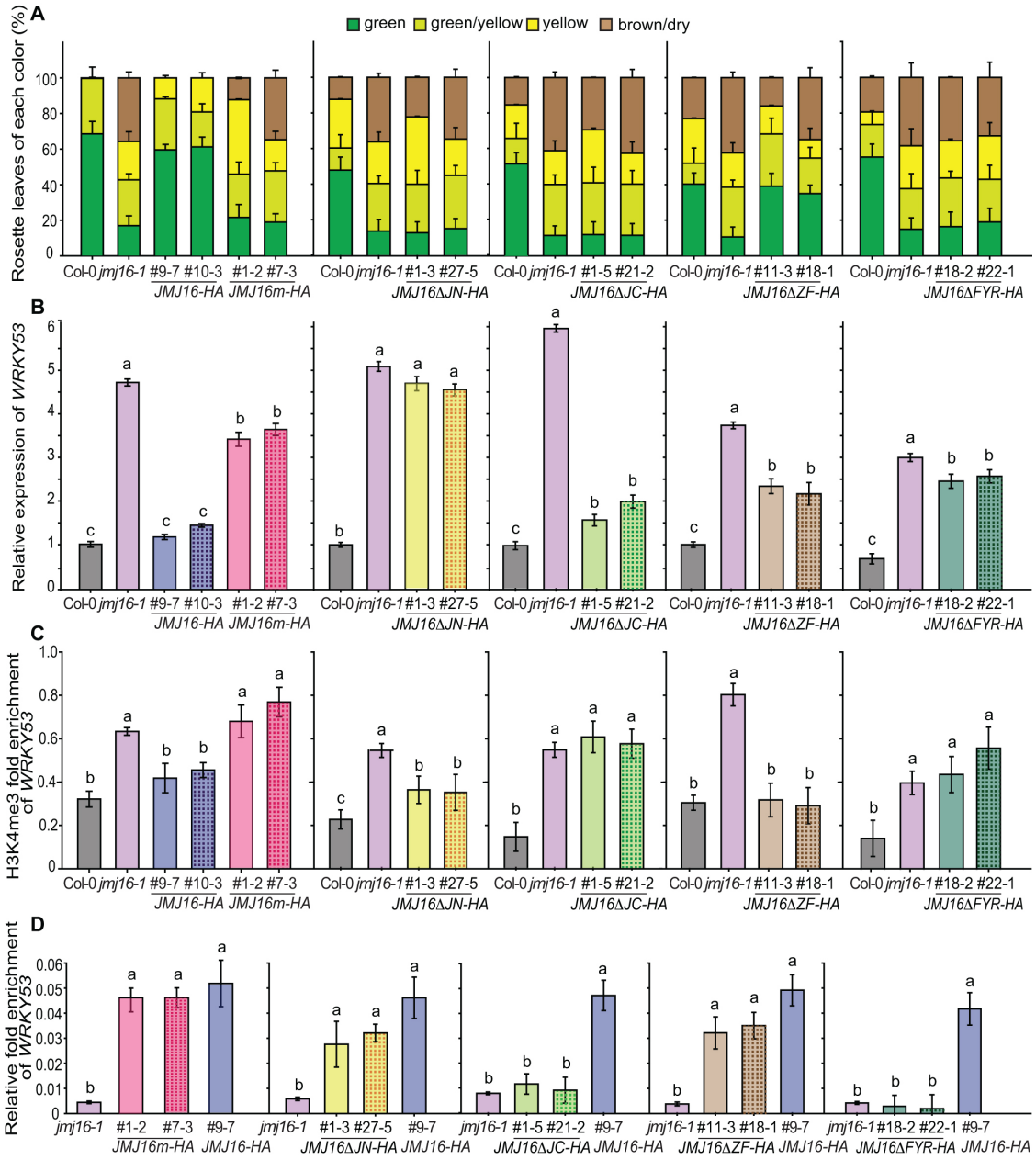

Figure 3. The demethylase activity and JmjN, JmjC, and FYR-rich domains of JMJ16 are required for the regulation of leaf senescence.

(A) Quantification of the leaf senescence phenotypes of 7-week-old plants grown under long-day conditions, as mentioned in **Supplemental Figure 2**. Error bars indicate ± SE.

(B) RT-qPCR analysis of *WRKY53* expression levels. *eIF4a* was used as an internal control.

(C) ChIP-qPCR analysis of H3K4me3 methylation status at the *WRKY53* locus. Anti-H3 and actin were used as internal references for ChIP-qPCR.

(D) ChIP-qPCR analysis of the association of JMJ16-HA and its mutant proteins with the *WRKY53* locus. A specific primer corresponding to the *WRKY53* R1 region (indicated in **Figure 4**) was used in the ChIP-qPCR analysis. Actin was used as an internal control.

Different letters indicate significant differences among genotypes based on one-way ANOVA with Tukey's honestly significant difference test ($P < 0.0001$).

Leaves 5 and 6 of 5-week-old long-day-grown plants were used for RT-qPCR and ChIP-qPCR analyses. Error bars represent ± SD (n=3).

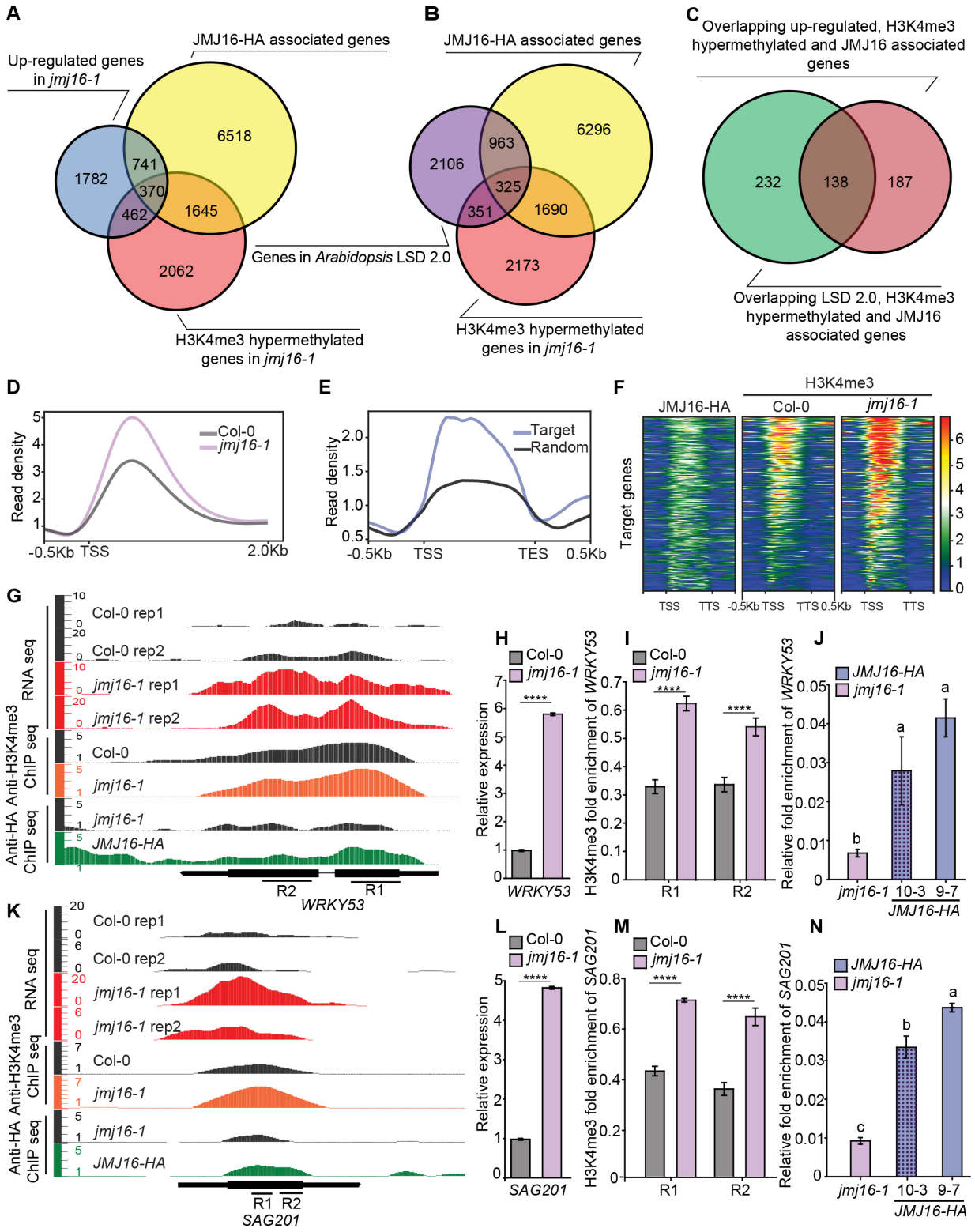

Figure 4. The transcription and H3K4me3 methylation levels of many SAGs are upregulated in *jmj16-1.*
(A) Venn diagram showing the overlap among genes that are transcriptionally up-regulated in *jmj16-1,* H3K4me3 hypermethylated genes in *jmj16-1* and JMJ16-HA associated genes.
(B) Venn diagram showing the overlap among SAGs from Arabidopsis LSD2.0, H3K4me3 hypermethylated genes in

jmj16-1 and JMJ16-HA associated genes.
(C) Venn diagram showing the significant overlap (Fisher's exact test, p-value = 9.64E-178) between the 370 targets from **(A)** and the 325 targets from **(B)**.
(D) Normalized read density of H3K4me3 ChIP-seq signals at the TSS of JMJ16 target genes in Col-0 and *jmj16-1*.
(E) Normalized read density of JMJ16-HA ChIP-seq signals in the gene bodies of JMJ16 target genes and the same number of randomly selected genes.
(F) Heatmaps of the gene body regions of JMJ16 target genes ranked by H3K4me3 levels in *jmj16-1*, showing concordant pattern of ChIP-seq signals of JMJ16-HA and H3K4me3 in Col-0 and *jmj16-1*.
(G) and **(K)** Genome tracks of RNA-seq, anti-H3K4me3 and anti-HA ChIP-seq data for *WRKY53* **(G)** and *SAG201* **(K)** loci in Col-0, *jmj16-1* and *JMJ16-HA* plants. Structures of *WRKY53* and *SAG201.* R1 and R2, specific regions used for ChIP-qPCR analysis. Y axis value means normalized read counts.
(H) and **(L)** RT-qPCR analysis of *WRKY53* **(H)** and *SAG201* **(L)** expression levels. *eIF4a* was used as an internal control. Error bars represent ± SD (n=3). Significant difference between Col-0 and *jmj16-1* was determined by Student's *t*-test (****: $P < 0.0001$).
(I) and **(M)** ChIP-qPCR analysis of H3K4me3 methylation status at the *WRKY53* **(I)** and *SAG201* **(M)** loci. Anti-H3 and actin were used as internal references for ChIP-qPCR. Significant difference between Col-0 and *jmj16-1 w*as determined by Student's *t*-test (****: $P < 0.0001$).
(J) and **(N)** ChIP-qPCR analysis of the association of JMJ16-HA with the *WRKY53* **(J)** and *SAG201* **(N)** locus. Specific primers corresponding to the *WRKY53* R1 region and *SAG201* R2 region were used in the ChIP-qPCR analysis. Actin was used as an internal control. Different letters indicate significant differences among genotypes based on one-way ANOVA with Tukey's honestly significant difference test ($P < 0.0001$).
Leaves 5 and 6 of 5-week-old long-day-grown Col-0, *jmj16-1,* and *JMJ16-HA* plants were used for RNA-seq, ChIP-seq, qRT-PCR, or ChIP-qPCR analyses. Error bars represent ± SD (n=3).

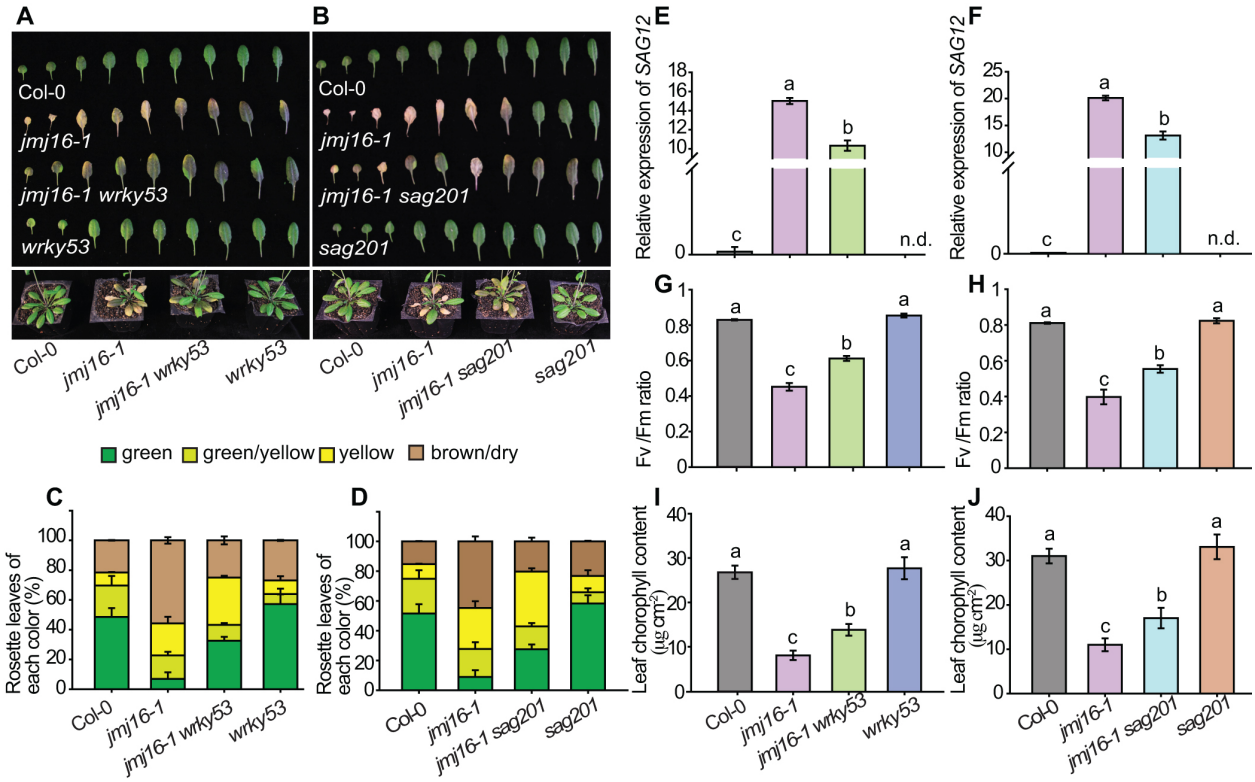

Figure 5. JMJ16 negatively regulates leaf senescence at least partly through *WRKY53* and *SAG201*.
(A) and **(B)** *wrky53* **(A)** and *sag201* **(B)** mutations partially suppressed the early-senescence phenotype of *jmj16*. Leaf senescence phenotypes of 7-week-old plants grown under long-day conditions.
(C) and **(D)** Quantification of the leaf senescence phenotype of 7-week-old plants grown under long-day conditions, as mentioned in **Supplemental Figure 2**. The means from three independent experiments and 15 plants were determined in each experiment. Error bars indicate ± SE.
(E) to **(J)** Expression level of *SAG12* **(E** and **F)**, Fv/Fm ratio **(G** and **H)** and Chlorophyll content **(I** and **J)** in leaves 5 and 6 of 6.5-week-old plants. Relative expression was normalized to that of *eIF4a*. Error bars represent ± SD (n=3). Different letters indicate significant differences among genotypes based on one-way ANOVA with Tukey's honestly significant difference test ($P < 0.0001$; n.d. indicates not detected).

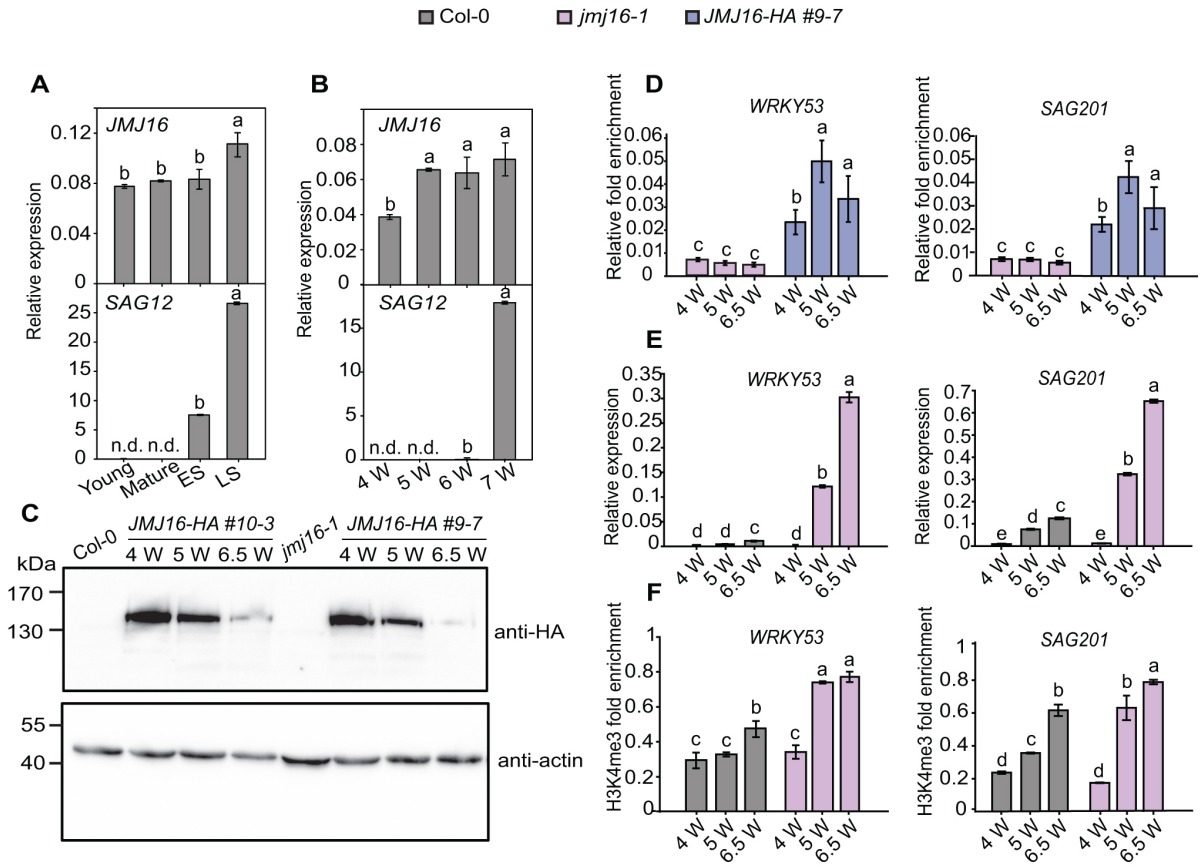

Figure 6. JMJ16 regulates SAG expression in an age-dependent manner.
(A) Expression levels of *JMJ16* and *SAG12* in the leaves of long-day-grown wild-type plants at the indicated developmental stages. Young: non-senescent and not fully expanded leaves; Mature: non-senescent and fully expanded leaves; ES: early senescing stage leaves; LS: late senescing stage leaves. Relative expression was normalized to that of *eIF4a*. Error bars represent ± SD (n=3).
(B) Expression levels of *JMJ16* and *SAG12* in leaves 5 and 6 of long-day-grown wild-type plants at the indicated developmental stages. Relative expression was normalized to that of *eIF4a*. Error bars represent ± SD (n=3).
(C) JMJ16-HA protein levels in leaves 5 and 6 of long-day-grown *JMJ16-HA* (#9-7 and #10-3) transgenic plants at the indicated developmental stages. Total protein extracts isolated from Col-0 or *jmj16-1* were used as negative controls. Anti-actin (EASYBIO BE0027) was used as a loading control. Anti-HA antibody (Sigma H6908) was used to detect JMJ16-HA. *JMJ16-HA* indicates the expression of *JMJ16-HA* driven by the *JMJ16* promoter in *jmj16-1*. 4 W, 5 W, and 6.5 W indicate 4-, 5-, and 6.5-week-old plants grown under long-day conditions, respectively.
(D) ChIP-qPCR analysis of the association of JMJ16-HA with the *WRKY53* (left) and *SAG201* (right) loci at the indicated developmental stages. Specific primers corresponding to the *WRKY53* R1 region and *SAG201* R2 region (indicated in Figure 3) were used in the ChIP-qPCR analysis. Actin was used as an internal control. Leaves 5 and 6 of *jmj16-1* and *JMJ16-HA* plants were used for analyses. Error bars represent ± SD (n=3).
(E) RT-qPCR analysis of *WRKY53* (left) and *SAG201* (right) transcript levels. *eIF4a* was used as an internal control.
(F) ChIP-qPCR analysis of the H3K4me3 methylation status at the *WRKY53* (left) and *SAG201* (right) loci. Anti-H3 and actin were used as internal references for ChIP-qPCR. Leaves 5 and 6 of long-day-grown Col-0 and *jmj16-1* plants at the indicated developmental stages were used in the RT-qPCR and ChIP-qPCR analyses. Error bars represent ± SD (n=3).
Different letters indicate significant differences based on one-way ANOVA with Tukey's honestly significant difference test ($P < 0.0001$; n.d. indicates not detected).